Fabrication and characterization of microsieve electrode array (μSEA) enabling cell positioning on 3D electrodes

IOP Publishing Journal of Micromechanics and Microengineering

J. Micromech. Microeng. **27** (2017) 015017 (16pp) doi:10.1088/0960-1317/27/1/015017

Fabrication and characterization of microsieve electrode array (μSEA) enabling cell positioning on 3D electrodes

B Schurink[1], R M Tiggelaar[1] J G E Gardeniers[1] and R Luttge[1,2]

[1] Mesoscale Chemical Systems, MESA+ Institute for Nanotechnology, University of Twente, PO Box 217, 7500 AE, Enschede, The Netherlands
[2] Microsystems, Department of Mechanical Engineering, Eindhoven University of Technology, PO Box 513, 5600 MB, Eindhoven, The Netherlands

E-mail: b.schurink@utwente.nl

Received 2 June 2016, revised 29 September 2016
Accepted for publication 20 October 2016
Published 16 November 2016

Abstract

Here the fabrication and characterization of a novel microelectrode array for electrophysiology applications is described, termed a micro sieve electrode array (μSEA). This silicon based μSEA device allows for hydrodynamic parallel positioning of single cells on 3D electrodes realized on the walls of inverted pyramidal shaped pores. To realize the μSEA, a previously realized silicon sieving structure is provided with a patterned boron doped poly-silicon, connecting the contact electrodes with the 3D sensing electrodes in the pores. A LPCVD silicon-rich silicon nitride layer was used as insulation. The selective opening of this insulation layer at the ends of the wiring lines allows to generate well-defined contact and sensing electrodes according to the layout used in commercial microelectrode array readers. The main challenge lays in the simultaneously selective etching of material at both the planar surface (contact electrode) as well as in the sieving structure containing the (3D) pores (sensing electrodes). For the generation of 3D electrodes in the pores a self-aligning technique was developed using the pore geometry to our advantage. This technique, based on sacrificial layer etching, allows for the fine tuning of the sensing electrode surface area and thus supports the positioning and coupling of single cells on the electrode surface in relation to the cell size. Furthermore, a self-aligning silicide is formed on the sensing electrodes to favour the electrical properties.

Experiments were performed to demonstrate the working principle of the μSEA using different types of neuronal cells. Capture efficiency in the pores was $>$70% with a 70% survival rate of the cell maintained for up to 14 DIV.

The $TiSi_2$–boron-doped-poly-silicon sensing electrodes of the μSEA were characterized, which indicated noise levels of <15 μV and impedance values of 360 kΩ. These findings potentially allow for future electrophysiological measurements using the μSEA.

Keywords: microelectrode, 3D electrode, 3D lithography, cell positioning, array, microsieve, microelectrode array

S Online supplementary data available from stacks.iop.org/JMM/27/015017/mmedia

(Some figures may appear in colour only in the online journal)

1. Introduction

A decade after the development of microfabrication techniques for micro-electro-mechanical-systems (MEMS), electrical sensors were integrated onto planar surfaces to realize the first microelectrode array (MEA) for extracellular reading of neurons in cultured neuronal networks. Such MEA platforms are a frequently used tool for *in vitro* electrophysiology and particularly in the neurosciences. They offer non-invasive, repeatable and long term monitoring of spontaneous activity, plasticity, and screening of the effects of chemical and electrical cues on the neurophysiological response the cultured network or brain slices [1]. Additionally, MEAs are used for high throughput drug development and toxicology studies [2–4]. Common MEA designs for dissociated cells rely on random seeding of cells on top of the surface of a chip encompassing planar electrodes. Consequently, the cells form a dense layer on the electrode array in a 2D fashion [5]. However, such setup complicates distinction of neurons coupled to the microelectrodes and complicated the distinction of active neurons from passive ones sharing the same electrode, which in fact limits the reproducibility, controllability and information being gained by means of this experiment. These limitations of a conventional MEA can be resolved by the positioning of cells by means of electrokinetic or hydrodynamic flow, which allows a novel type of electrophysiology assay to be developed. A hydrodynamic flow design can be realized by side channels originating from a main channel, where the side channels allow for fluid flow, yet have dimensions smaller compared to the size of the cell [6–8]. Such hydrodynamic positioning method can be transferred to an array with integrated microelectrodes, to realize a so-called microchannel array (MCA) [9, 10]. Likewise, by applying the same principle, a membrane can be utilized to realize patch-clamp devices in which a high resistance seal is formed between the cell membrane and the surface of the membrane pore [11–13]. Although both the MCA and membrane patch-clamp allow for high throughput positioning and recording of single cells, the microenvironment onto which the cells are positioned and are expected to adhere consists of a planar surface comparable to that of the conventional 2D MEA, which essentially resembles a petri dish cell culture. Such 2D models are shown to be less physiological relevant compared to the state-of-the-art 3D cultured neurons, whereby even a few cell layers in artificial matrix in a so called microtunnel or fluidic channel can already make a substantial difference [14–16]. Moreover, other 3D applications have been presented in MEA technology, mainly concerning the electrode geometry [5]. Spiked or mushroom shaped electrodes have been fabricated which can be engulfed by a neuron to achieve an increase in the electric coupling compared to the 2D electrode, thus a potential higher spatial resolution can be obtained. To a different end, spiked electrodes have been designed to penetrate the first layer of dead cells of brain tissue slices, decreasing the distance between live cells and the electrodes. In contrast to these out-of-plane electrode structures, in this work we utilize in-plane structures to achieve a 3D microenvironment and 3D electrodes for electrophoresis, but also allow for cell positioning using hydrodynamic flow, which is not feasible with the design of spiked or mushroom shaped 3D electrodes.

We hypothesis that the in-plane 3D microenvironment allows cells to adhere and to maintain their sphere-type morphology [17], and by integrating electrodes at these locations a new type of information signals can be obtained which is more comparable to the *in vivo* situation, as indirectly has been demonstrated in recent literature [18]. Also, the in-plane structures allows positioning of single neurons on the microelectrodes and thus permits the distinction of neurons and enables single-unit recordings in contrast to multi-unit recordings as often observed in commercial MEA devices. This ability towards single neuron positioning is supported by preliminary work [19], in which hydrodynamic positioning of cells is governed to a single cell in a single pore. Essentially, a positioned cell ‘clogs’ its pore, thereby reducing the flow through the pore (aperture) and thus preventing other cells from being positioned in the same pore.

To provide the tool to prove this hypothesis, a silicon sieving structure (figure 1(a)) has been realized by us previously [20], which contains 900 inverted in-plane pyramidal-shaped pores with pore openings of a 20 μm side length at the top. The square aperture at the bottom of each these pores is highly uniform for each fabricated sieving structure and its size is depending on the etch time. The pyramidal shape of each pore, and thus the inclined sidewalls, are the result of an anisotropic wet etch micromachining process of single crystalline silicon. Furthermore, these pores are arranged in form of an orthogonal array of which subsequently 60 pores can be functionalized with an individual addressable electrode according to the format of standardized MEA reader (Multi Channel Systems, Reutlingen, Germany).

In case neurons are positioned in each of these pores, these electrode–neuron interfaces, can function as transducers to establish a neuroelectronic interface for a larger network of neurons grown atop of the microsieve structure, which can be realized by the use of a previously developed bioreactor [21].

In this work, the design and fabrication process of such a new neuroelectronic interface, the microsieve electrode array (μSEA) is presented. To this end, we also discuss the various efforts to optimize photolithography atop of the previously realized silicon sieving structure and present a novel engineering solution for a selective etch step for both the planar surface as well as the walls of the inverted pyramidal-shaped pores at the same time. This solution allows for the selective removal of a previously deposited uniform layer of insulation material from solely the contact and sensing electrodes, thus preserving the insulation on the electrical wires (figure 2). Hereby a novel self-aligned 3D electrode process is realized which supports the fine tuning of the sensing electrode surface and location on the pore wall to allow for distinction of specific cell types positioned according to their cell size. Furthermore, we also demonstrate the initial microfluidics for the cell positioning, the cell biological properties and electrical characterization of the function of this novel brain-on-chip platform technology.

We demonstrate the full fabrication concept of the μSEA including the integration and isolation of electrode material

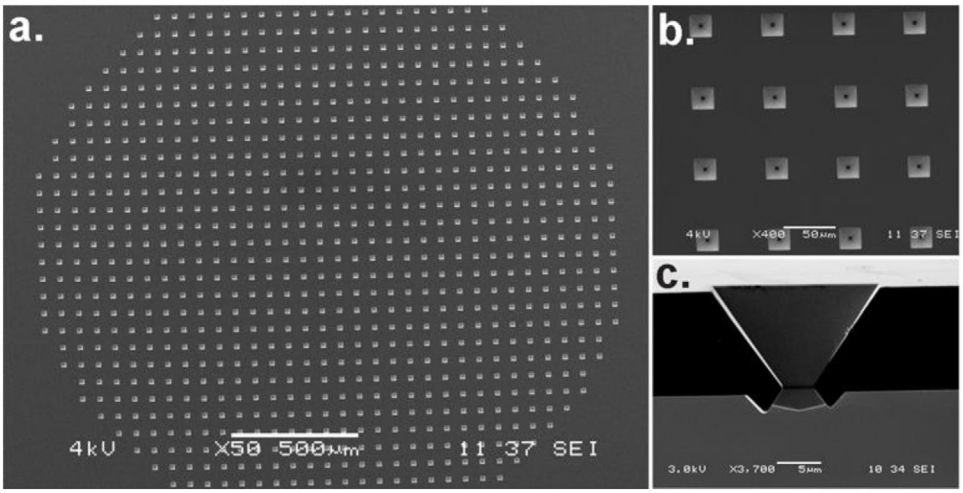

Figure 1. Scanning electron microscope images of the top side of the silicon sieving structure, featuring 900 pyramidal pores in a circular area with a radius of 1.2 mm (a). The pores have a base length of 20 μm and are distributed with a 70 μm pitch (b). The circular area containing the pores has a thickness of approximately 16 μm and each pore has a highly uniform pore aperture of 3.2 μm and presents a sleeve structure at the bottom side of the sieving structure, as a remainder from deep anisotropic backside etching to realize the sieving structure. The exact size of each sleeve structure depends on the location of the pore in the circular area of the sieving structure [19]. Sleeve structures with the largest size are located at the peripheral location of the sieving structure (c).

on the silicon sieving structure to complement the electrical readout function and fabrication of sensing electrodes inside of the pores.

2. Materials and methods

In figure 2 the schematics of the μSEA is depicted to illustrate the layout of the electrodes and lead wires, including the electrical insulation and its removal which is described in detail in section 2.3.

Figure 3 shows the fabrication process steps for integrating the electrodes in the sieving structure, which results in a fully functionalized μSEA. In the following subsections the various process steps are described in more detail.

2.1. Patterning of the electrode material

After realizing the sieving structure in the center of a double-side polished 4-inch (1 0 0)-silicon substrate, a silicon-rich silicon nitride (SiRN) layer of 250 nm (figure 3(a)) is deposited by low pressure chemical vapor deposition (LPCVD, 60 min, 850 °C). A poly-silicon (poly-Si) layer of 220 nm is also deposited by LPCVD (80 min, 590 °C or 620 °C) and subsequently dry thermal oxidation (45 min, 950 °C) is performed to grow 25 nm of oxide (figure 3(b)). Photolithography is performed on the top side, including spin coating (4000 rpm, 30 s) of HMDS (hexamethyldisilazane; adhesion promotor) and OiR 906-12 resist (Arch Chemicals), pre-baking at 95 °C for 1 min and UV exposure (12 mW cm^{-2}) for 4 s (EVG 620 mask aligner). Post to flood exposure of the back side (20 s) of the sample, the substrate is developed in Olin OPD 4262 developer solution (Arch Chemicals), to define the electrodes and lead wire pattern in the photoresist (figure 3(c)). Subsequently, the non-masked oxide layer is removed in buffered hydrofluoric acid (BHF solution, 1:7, 40 s) (figure 3(d)). Subsequently,

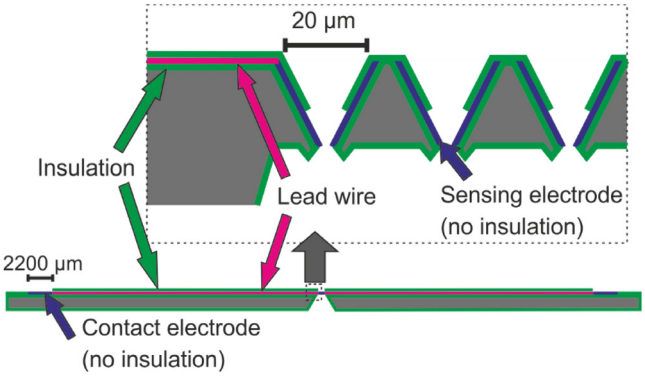

Figure 2. Schematic illustration of the cross section of the μSEA, presenting the layout including insulation layers, contact electrodes, sensing electrodes and the lead wires for connecting each contact electrode with a sensing electrode. The insulation layer deposited on top of the electrodes and lead wires is locally removed from both the contact and sensing electrodes.

the resist is stripped in nitric acid and then the exposed poly-silicon is removed with tetramethylammonium hydroxide (25% TMAH, 1 min, 70 °C) through the selectively opened oxide masking layer. Finally, the residual oxide is removed with BHF to access the patterned poly-silicon (figure 3(e)).

2.2. Doping of the poly-silicon

The patterned poly-Si is boron doped (figure 3(f)) by means of solid source dotation (SSD). To provide the μSEA with boron-doped poly-Si of a low resistivity, various poly-Si deposition temperatures and SSD-settings were explored. Poly-silicon films of 220 nm were deposited at 590 °C and 620 °C, and subsequently boron drive-in was performed at temperatures of 950 °C, 1000 °C and 1050 °C for 15, 30 and 60 min, respectively. The boron oxide layer, formed during the SSD process [22], is etched in BHF (10 min), followed by an oxidation step

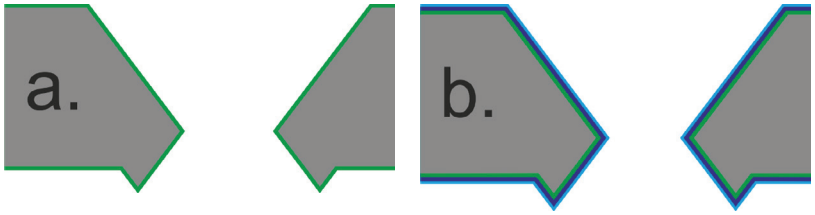

The silicon sieving structure is provided with a silicon nitride layer (a), poly-Si is deposited and thermally oxidized (b).

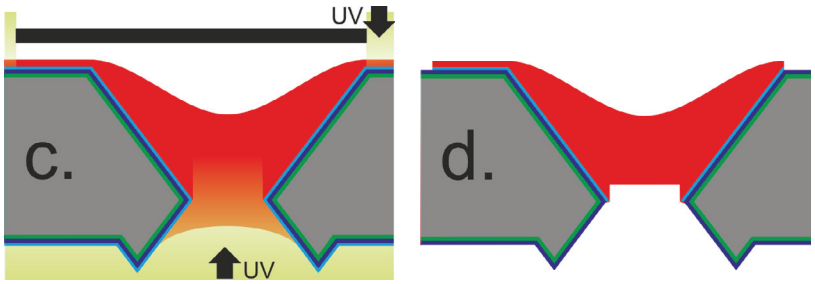

Photoresist in spin coated on the surface, coating the pore walls and sleeve structures. UV exposure through a mask on the top side results in the pattern of the sensing electrodes, lead wires and contact electrodes. Next, a flood exposure is performed from the back side of the sample to remove the resist at the 'sleeve structures' and subsequently the resist is developed (c). The oxide is patterned by BHF etching (d).

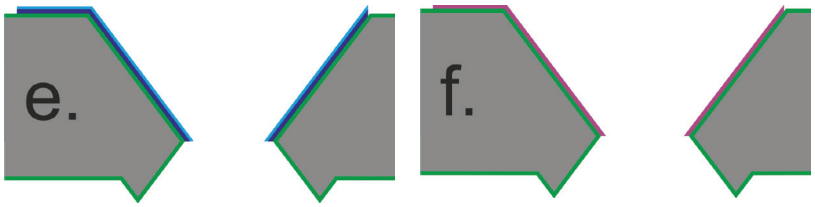

The photoresist is removed and the poly-Si is patterned by TMAH etching (e). After removal of the oxide layer by BHF, the poly-Si is boron doped by means of solid source dotation (f).

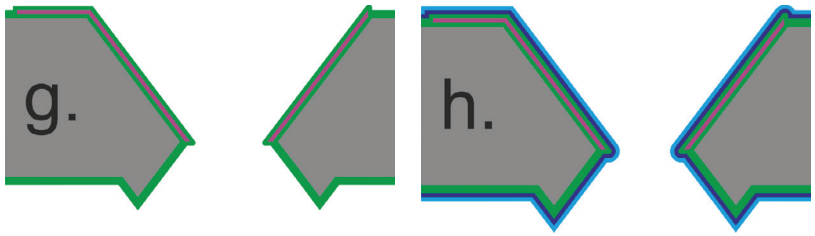

A second silicon nitride layer is deposited to cap the boron doped poly-Si electrode layer (g). Then a sacrificial poly-Si layer is deposited and thermally oxidized (h).

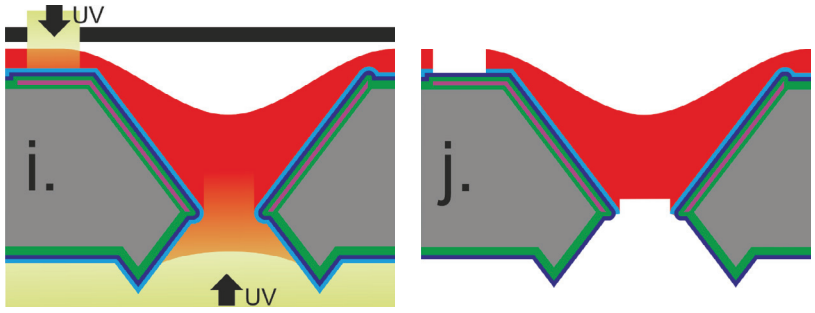

Photolithography is performed using a mask containing the contact electrodes, followed by a flood exposure of the back side of the sample (i). Subsequently, the oxide at the contact electrodes and backside of the sample is etched by BHF (j).

Figure 3. Schematic illustration of the fabrication process of a sensing electrode in a single pore, located at peripheral region of the sieving structure, in accordance with the cross-section in figure 1(c).

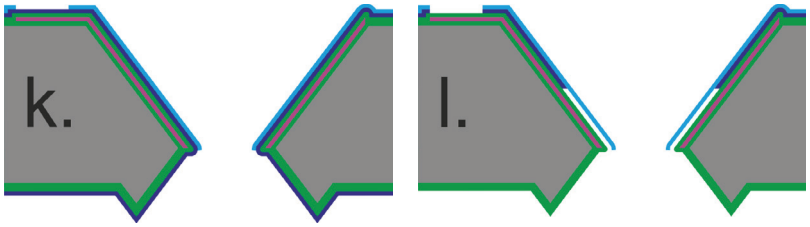

The resist is removed (k) and TMAH is used to etch the poly-silicon at the contact electrodes, the backside of the sample and from underneath the oxide layer at the sensing electrode (l).

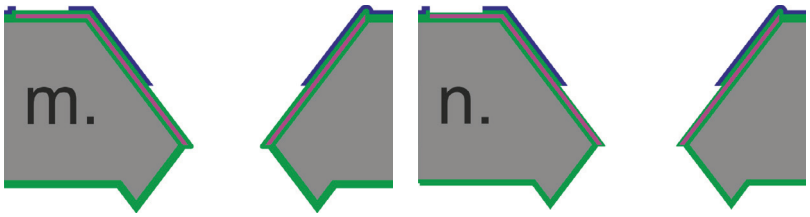

The oxide layer is removed in BHF (m) and the silicon nitride layer is time-stop etched in 50% hydrofluoric acid until a thin layer is left (n).

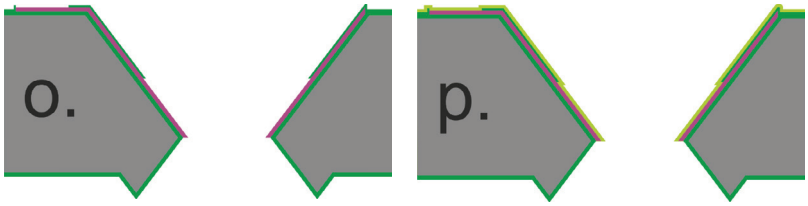

The poly-Si layer is removed in TMAH and the thin silicon nitride layer removed in 50% hydrofluoric acid to access the boron doped poly-Si contact electrodes and sensing electrode (o). A titanium layer is sputtered on the top side of the sample (p).

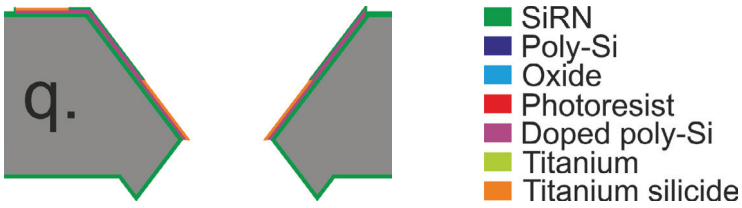

Rapid thermal processing and selective RCA-1 (Radio Corporation of America) etching are performed for the formation titanium silicide at the doped poly-Si and titanium interface (q).

Figure 3. (*Continued*)

at 800 °C to 'crack' a thin B_3O_5/poly-Si layer. The hereby formed oxide layer is removed in BHF (10 min).

2.3. Patterning of the SiRN isolation layer

After the SSD process, the substrate featuring the patterned and doped poly-Si—which form the contact electrodes, the lead wires and the sensing electrodes—is electrically isolated with SiRN (60 min, 850 °C; 250 nm) (figure 3(g)). This SiRN isolation layer has to be selectively removed to realize the contact and sensing electrodes. To achieve this, a masking poly-Si (60 min, 590 °C, 180 nm) layer is applied, which is wet-thermally oxidized (16 min, 950 °C) to grow a layer of 150 nm oxide (figure 3(h)), reducing the poly-Si layer to a thickness of 110 nm. Next, a layer of HDMS and OiR 907-17 photoresist (Arch Chemicals) is spin coated (4000 rpm) on the surface, pre-baked at 95 °C for 1 min and exposed by UV (12 mW cm^{-2}) for 6 s (EVG 620 mask aligner) through a mask containing the contact electrodes. Additionally, the backside of the sample is flood exposed for 20 s by UV light (figure 3(i)), followed by development of the resist using Olin OPD 4262 developer solution (Arch Chemicals), hereby removing all UV exposed resist from the oxide layer. The exposed oxide (at the contact electrodes and the complete backside of the sample) is removed by BHF (1 min) (figure 3(j)). The resist is stripped in nitric acid (figure 3(k)), and subsequently the exposed poly-silicon at the contact electrodes and backside of the sample is selectively etched in 25% TMAH (1 min, 70 °C) using the oxide layer as a mask. At this point, upon continuing the TMAH etch, the poly-Si is sacrificially etched from underneath the oxide, starting at the pore aperture and continuing along the pore walls (figure 3(l)). It has to be noted that the time duration of this TMAH under-etch step eventually determines the size of the sensing electrode. Once the poly-Si is under-etched to the desired dimensions, the residual oxide layer is removed using BHF (1 min) (figure 3(m)). The exposed SiRN is then wet-etched in 50% hydrofluoric acid (HF; 50 min) using the poly-Si layer as mask, until a thin layer of approximately 20 nm of SiRN is preserved on the doped poly-Si (figure 3(n)). The thickness of this SiRN layer is

measured by ellipsometry (Woollam M-2000UI) and prevents the etching of the boron doped poly-Si electrode layer, as the masking poly-Si layer has still to be removed by 25% TMAH (2 min). Next, a 50% HF etch (5 min) is done to remove the remaining 20 nm of SiRN from the entire sample, hereby accessing the doped poly-Si electrodes (figure 3(o)).

2.4. Formation of low resistivity $TiSi_2$ on the sensing electrodes and dicing

After SiRN is removed from the contact electrodes and the sensing electrode area, native oxide is removed from the doped poly-Si with 1% hydrofluoric acid (HF) dip and a thin-film of titanium (80 nm) is sputtered (figure 3(p)). To form the low resistivity titanium silicide (C54–$TiSi_2$) only at the interface of poly-Si and titanium, a double step rapid thermal processing (SSI Inc., Solaris 150) is performed (figure 3(q)). A first Rapid Thermal Anneal 1 (RTP1) step is done under either nitrogen or forming gas (95% argon and 5% hydrogen) with a ramping temperature rate of 50 °C s^{-1}–550 °C, 650 °C, 700 °C or 750 °C, and once the desired temperature is reached it is kept at this temperature for 30 s. During this step the C49 phase $TiSi_2$ is formed. A so called RCA-1 (Radio Corporation of America) etch, consisting of a mixture of hydrogen peroxide (H_2O_2), ammonium hydroxide (NH_4OH) and water (H_2O) (1:1:5) is performed (15 min), which removes the non-reacted titanium and the side products, such as titanium nitride and titanium oxide. A second rapid thermal anneal 2 (RTP2) is performed under nitrogen at a temperature of 850 °C for 30 s, which is reached with a ramp rate of 50 °C s^{-1}. Hereby the C49 phase is converted into the desired low resistivity C54 phase [23]. To verify the formation of C54 phase titanium silicide at the locations of the sensing electrodes, energy-dispersive x-ray spectroscopy (EDX) analysis is utilized integrated within a SEM instrumentation (Merlin HR-SEM, Zeiss). EDX analysis is performed 2 d after the formation of the titanium silicide.

Finally, the μSEA, with a footprint of 49 mm × 49 mm, is diced from the 4 inch substrate. Here, UV-foil (Adwil 210) is applied on both sides to protect the μSEA during dicing (DISCO DAD 321). Before applying the dicing foil, a dummy piece of silicon is placed on the location of the sieving structure, which prevents damage to the sieving structure upon removal of the dicing foil.

2.5. Size and shape of the poly-Si sensing electrode in the μSEA

In the μSEA fabrication process, boron doped poly-Si is used as electrode material, which is patterned on the planar surface to form square contact electrodes with a width of 2200 μm, lead wires with a decreasing width of resp. 200, 120, 30 and 10 μm, as well as size and shape tunable sensing electrodes inside the pores. In more detail, the sensing electrodes consist of electrode material patterned in the pyramidal pores on its four walls up to a certain height, which might give rise to redundant electrode surface area. The upper pore opening in the fabricated μSEA was fixed to at 20 μm, which was selected based on the average size of a mammalian cell in solution (10 μm). After complete insulation of the sample surface by SiRN, the contact electrodes and only a part of the boron doped poly-Si in the pores are revealed (the sensing electrode) by locally removing this insulation. In the following, the principle of insulation removal by sacrificial layer etching will be shown for only the sensing electrode, as this approach has no significant effect on the size of the contact electrodes due to their relative large size (2200 × 2200 μm, depicted in figure 2), whereas it has a large influence on the size, shape and surface area of the final sensing electrode. The tuning of the sensing electrode can be done using two time-stopped etch steps during the μSEA fabrication process. The first time-stopped etch step (ET_1) (figure 3(e)) comprises the patterning of the poly-Si and the second time-stopped etch step (ET_2) (figure 3(l)) comprises the removal of the SiRN insulation layer by sacrificial layer wet etching, as described in detail in subsection 2.3.

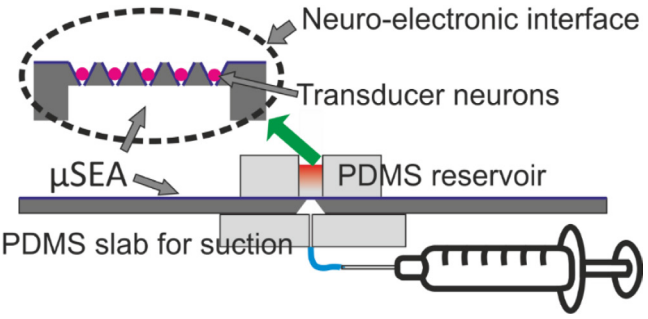

Figure 4. Schematic illustration of the positioning of transducer neurons on the sensing electrodes, establishing the neuro-electronic interface. The PDMS reservoir and PDMS slab are adhered on either side of the μSEA device. Dissociated neurons in 10 μl are brought on top of 50 μl culture medium in the PDMS reservoir. Suction is applied by means of a syringe, reducing the volume in the PDMS reservoir to 10 μl.

2.6. Positioning of μSEA transducer neurons

The positioning of the so called 'transducer neurons' in the pores of the μSEA was studied using three cell types. The used cell types are rat cortical neurons, SH-SY5Y cells and rat hippocampal cells. Prior to positioning cells, the μSEA was sandwiched in between two PDMS slabs, with dimensions of 30 × 20 × 5 mm (length, width and height). Before adhering the PDMS slab to the μSEA at the top it was punched with a diameter of 8 mm to form a reservoir. On the back side of the μSEA, a PDMS slab was attached that was punched with a diameter of 0.6 mm to connect a tube fitting to a capillary with 0.5 mm diameter and a length of 100 mm coupled to a 1 ml syringe (figure 4).

Prior to mounting the PDMS slabs to the μSEA, all parts were disinfected with 70% ethanol and rinsed with phosphate buffered saline (PBS). A volume of 50 μl culture medium was pipetted into the reservoir before transducer cell positioning. The used transducer cells were rat cortical neurons in R12 enriched culture medium [24], SH-SY5Y cells in Dulbecco's modified eagle medium (DMEM) with retinoic acid [25] or hippocampal neuronal cells in Neurobasal medium [26]. The

cortical and SH-SY5Y were diluted to a density of 100 cells μl^{-1}, respectively 10 μl of the cell solution (approximately 1000 cells) was added on top of the already present 50 μl culture medium using a micropipette. Suction was applied by the syringe (1 ml) for 30 s, facilitating a flow through the apertures of the μSEA device until the culture medium in the reservoir is reduced by 50 μl. This leads to positioning of the transducer cells into the pyramidal pores that contain the sensing electrodes. Of the used transducer cells, cortical neurons were positioned and stained with a LIVE/DEAD® assay (Sigma Aldrich) 2 h after positioning. Images were taken by a fluorescence microscope (Leica, DM IL LED). Transducer cell positioning efficiency was studied for cortical and SH-SY5Y cells, respectively, which were stained by Green CMFDA Dye (CellTracker) directly after positioning. The seeding efficiency was calculated for the number of occupied pores in the μSEA in relation to the total number of pores.

The hippocampal neuronal cells were diluted to 6000 cells μl^{-1} and were presented in the reservoir in the already present 50 μl culture medium. For this experiment no suction was applied in order to test the biocompatibility of the μSEA surface on this specific cell type.

Unstained transducer cells (rat cortical, SH-SY5Y and hippocampal cells) were provided with 50 μl of their specific culture medium, which was refreshed each other day for further cell culturing, for the duration of 14, 7 and 21 d, respectively.

In agreement to the used sieve cross flow used for the positioning of transducer neurons, a model in COMSOL software is realized to obtain an indication of the amount of shear stress at the walls of individual pores during positioning of the cells. The data was obtained for a flow of 0.1 ml min^{-1}, which is identical to the positioning experiments, in which 50 μl is flown through the 900 pore apertures of the sieving structure in 30 s.

2.7. Culturing and analysis of μSEA transducer neurons

All transducer cells were cultured by refreshing the appropriate culture media every other day. The hippocampal neuronal cells were observed by light microscope at 10× magnification at 3, 10 and 21 d *in vitro* (DIV). The cortical cells were cultured for 14 DIV and the SH-SY5Y cells were cultured for 7 DIV. Both cortical and SH-SY5Y were prepared for scanning electron microscopy (SEM) analysis (JEOL JSM 5610) to study neuron morphology and neuronal processes. A standard protocol was used including fixation, dehydration and drying [27]. In brief, the μSEAs containing the cells were washed with PBS, fixated with 4% paraformaldehyde, washed with PBS and dehydrated with 70, 80 and 90% ethanol in PBS and 100% ethanol. After removal of the 100% ethanol, the samples were air dried by hexamethyldisilazane (HMDS) treatment. This step included adding HMDS in ethanol (1:2), replacing with HMDS in ethanol 2:1 and replacing with HMDS, which was air-dried. The SEM images were analyzed for the investigation of the neuronal processes and the resulting cell morphology.

2.8. μSEA electrical characterization

Three μSEAs (devices A, B and C) were used for electrical characterization, 25 d after titanium silicide formation. The impedances of the sensing electrodes in the μSEAs were measured using a setup consisting of a LCR meter (Hewlett Packard 4284A Precision) with four-terminal pair configuration for external wiring correction. Both PDMS parts (section 2.6) (including syringe) are adhered to the μSEA device, of which the reservoir is filled with 100 μl PBS. To wet the sensing electrodes, suction was applied by the syringe (1 ml) for 30 s, facilitating a flow of PBS through the apertures of the μSEA device until the PBS in the reservoir is roughly halved to 50 μl. Next, one pair of microprobes was positioned on the contact of the reference electrode and the other pair on the designated contact electrode of a sensing electrode (Ref to Sens). The influence of the reference electrode was studied by positioning one pair of microprobe tips directly in the PBS solution (present in the reservoir) and the other pair on the designated contact electrode of a sensing electrode (PBS to Sens). Impedance measurements were performed by applying a voltage amplitudes in a range of 0.1 V–2 V at a frequencies of 20 Hz–100 kHz. The electrode noise was measured by a FA60s filter amplifier and a C1060BC preamplifier (MultiChannelSystems GmbH, Reutlingen, Germany). The noise was measured after 5 min of signal stabilization. A homebuilt program (Labview software) was used for noise analysis and data collection. The noise of the 60 electrodes was averaged for each of the three μSEA devices.

3. Results and discussion

The results include various explorative results to better understand the process challenges and are discussed step by step in the following subsections.

3.1. Patterning of the electrode material

The silicon sieving structure has been realized in the center of a double-side polished 4-inch (100)-silicon substrate according to the previously reported process [20]. The surface of the substrate was isolated with a SiRN layer (figure 3(a)), on which the patterned electrode base material was realized (figures 3(b)–(e) and 5(a)–(c)). Poly-silicon as electrode material has a good compatibility with the SiRN isolation layer and enables high temperature processing for the used LPCVD technology, which is not possible with metal based electrodes [28]. Additionally, poly-Si is successfully patterned by wet etching steps, which is possible because of its excellent etch selectivity with respect to the majority of the employed LPCVD materials. The initial thickness of the poly-silicon (220 nm) is reduced to approximately 200 nm upon oxidation, since the oxidation process consumes part of the poly-silicon (i.e. in this case 20 nm).

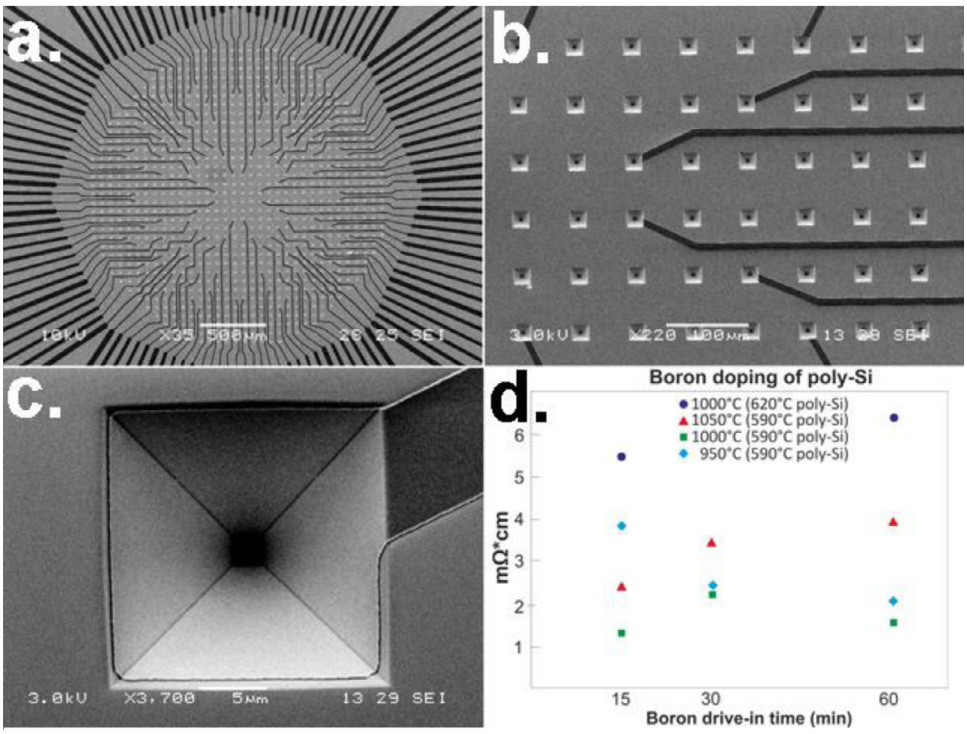

Figure 5. Scanning electron microscope images of the patterned and boron doped poly-silicon. The poly-silicon pattern forms the electrode layer (a) consisting of contact electrodes, lead wires (b) and sensing electrodes in the pyramidal shaped pores of the sieving structure (c). The poly-silicon is boron doped by means of solid source dotation at different drive-in temperatures and times (d). For boron doped 195 nm thick poly-Si electrode layer deposited at 590 °C the lowest resistivity is obtained for a drive-in temperature of 1000 °C for 15 min.

3.2. Doping of the poly-silicon

The patterned poly-Si is boron doped (figure 3(f)) to obtain low resistivity material. Various poly-Si deposition temperatures and SSD-settings were explored, of which the lowest resistivity was used for further processing. Poly-silicon films of 220 nm were deposited at 590 °C and 620 °C, and subsequently boron drive-in was done at temperatures of 1000 °C, for 15, 30 and 60 min. Electrical analysis indicated a significant lower resistivity for the poly-Si deposited 590 °C compared to the 620 °C, consequently, further optimization were performed using solely the poly-Si deposited at 590 °C. Here, the duration of the boron drive-in at each temperature (950 °C, 1000 °C and 1050 °C) was set to 15, 30 and 60 min. In figure 5(d) an overview of the measured resistivity are given per boron drive-in condition.

The best result was achieved with an initial 220 nm thick poly-Si film deposited at 590 °C and SSD boron-doping with drive-in settings of 1000 °C for 15 min. The resistivity of this layer was 1.33 mΩ cm (sheet resistance 78 Ω sq^{-1}), which is in agreement with similar doping efforts described in literature [22]. After boron doping, the poly-Si film has an average thickness of 195 nm, due to some silicon consumption during the SSD process due to the formation of boron oxide as dopant source.

3.3. Patterning of the SiRN isolation layer

After patterning and doping of the poly-Si layer, the applied SiRN isolating layer (figure 3(g)) has to be removed at the locations of the contact and sensing electrodes to ensure an electrical contact with the cultured neurons. The most straightforward approach is the use of photolithography similar to the process for patterning of poly-Si for the formation of the electrodes (described in paragraph 2.1, figures 3(c) and (d)). However, in contrast to the resist used for patterning of the poly-Si (first time-stopped etch), it is difficult to uniform expose a positive photoresist at the location of the inclined pore walls. Since the SiRN has to be removed only at the lower parts of the inclined walls of the pores, where eventually the transducer neurons adhere to the sensing electrode. Multiple problems were encountered in the trails to realize this selective removal of SiRN from the lower region of the pore walls using conventional standard UV photolithography techniques, mainly because conventional photolithography is a technique developed for obtaining patterns on 2D surfaces. Although non-satisfactory results were obtained using conventional UV photolithography techniques for the simultaneous removal of SiRN at the contact and sensing electrodes, the observed results can be valuable for other researchers who need to perform lithography on topographical structures—here anisotropic etched pores—and therefore experimental details are added to this publication as supporting information (stacks.iop.org/JMM/27/015017/mmedia).

In fact, for the successful removal of the SiRN from the inclined walls of the pores (sensing electrodes), a different lithography concept is developed, using the geometrical properties of the sieve as mask. This approach is based on wet etching of sacrificial layers and the physical connection of the top and bottom side of the sieving structure (figure 1(c)).

In more detail, LPCVD materials are deposited on both sides of the sieving structure, yet these materials can be selectively removed from both sides by a single process on the back side. Combined with the use of the sieving structure geometry, the pore apertures can be utilized to access and remove LPCVD material from the front side. With this concept, the size and shape of the sensing electrode is directly related to the duration of the time-stop etching step of the sacrificial layer and can thus be tuned. Such tuning of the electrode size/shape is an additional asset of this concept.

In practice, for this concept two techniques can be utilized to process only the back side of the sample (which allows for the selective removal of sacrificial poly-Si from both the front and back side), resp. the 'sacrificial layer dry etching' approach and the 'sacrificial layer photoresist' approach.

In the 'sacrificial layer dry etching' approach, described in more detail in the supporting information, two consecutive dry etch steps are utilized. Although this approach can be successfully applied for the selective removal of the SiRN insulation layer, the obtained sensing electrode surface was found not to be identical for all pores in the sieving structure, due to the difference in starting point of sacrificial layer etch.

In case of the 'sacrificial layer photoresist' approach (described in section 2.3), the entire surface in provided with an poly-Si layer, which is oxidized (figure 3(h)). The front side of the substrate is coated with photoresist, the sample is exposed at the locations of the contact electrodes and flood exposed by UV-light from the back side to remove photoresist present on the sleeve walls (figure 3(i)). In fact, the described problems (i.e. resist accumulation and limited UV penetration depth) of using photoresist and a photomask are not applicable to this approach, as no exposure of resist has to be performed on the pore walls. After development of the resist, the oxide is wet etched, removing the oxide from the back side of the sample (figure 3(j)). After back side processing (oxide etching), at the front side the resulting oxide layer exhibits a star-shaped opening in the pore (figures 3(k) and 6(a)). This is likely due to wetting effects of the relative thin oxide at the concave corners of the pore (in comparison to the pore walls) [29]. After the sacrificial poly-Si etch (figure 3(l)), the star-shaped opening changed to a clover shaped opening (figure 6(b)), indicating that poly-Si in the concave corners of the pore is etched at a (slightly) higher rate compared to the pore walls.

Comparing both approaches, the photoresist route has the advantage of etching multiple samples in one run, as well as that the contact electrodes and sensing electrodes can be accessed simultaneously. More important, photoresist route is non-depended on the sleeve structures (and hence the starting point of the poly-Si under-etch), thus yielding the smallest variation in sensing electrode surface area for the μSEA.

Once the sacrificial poly-Si is patterned as required (figure 3(m)), the SiRN mask is thinned by wet etching at the locations of the contact and sensing electrodes (figure 3(n)). A thin layer of SiRN ($\pm$20 nm) is preserved to protect the boron doped poly-Si electrode layer from the TMAH etchant, which is removed after dissolving the sacrificial poly-Si layer (figure 3(o)).

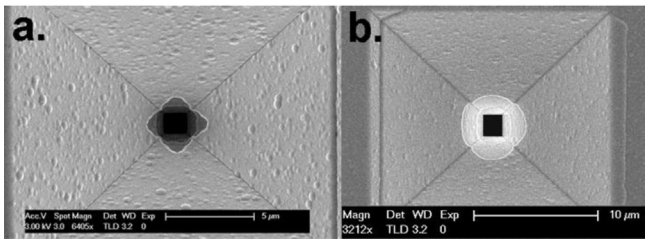

Figure 6. Scanning electron microscopy images of the wet etch approach. The oxide layer is wet etched according to the photoresist pattern on the bottom side of the sample (a), followed by removal of this oxide layer after the wet etching of the sacrificial poly-Si layer (b). The star-shaped opening in the oxide resulting from the oxide etch transfers into a clover-shaped opening after the poly-Si under-etch and this shape represents the sensing electrode.

3.4. Formation of low resistivity $TiSi_2$ on the sensing electrodes and dicing

Upon removal of SiRN, thereby exposing the boron doped poly-Si electrode material, a titanium silicide (C54–$TiSi_2$) could be formed by sputtering Ti, RTP and selective RCA etching (figures 3(p) and (q)). To ensure a good electrical signal transfer between the neuroelectronic interface and the readout equipment over time, the addition of a C54–$TiSi_2$ coating is preferred because of its ultra-low resistivity and a relative low oxidation rate during cell culturing compared to pure poly-Si [30]. Here, RTP was used instead of a heating furnace to minimize the dopant depletion and to prevent for oxidation of titanium after sputtering [31–34]. The temperature required to form the C49-phase $TiSi_2$ on boron doped poly-Si of the sensing electrodes by RTP was studied. The EDX spectra taken from the sensing electrodes show an increased concentration of titanium compared to the SiRN-isolated areas in-between the pores if RTP1 is carried out at a temperature of 700 and 750 °C. This result evidences that the salicide process is successful at the sensing electrodes in the pores, as well as that other titanium compounds are dissolved by the RCA-1 solution. Interestingly, at contact electrodes, which also feature a titanium/poly-silicon interface, no $TiSi_2$ is formed. It has to be noted that this is not a major issue, since the connecting pins of the external readout system will easily penetrate through any (native) oxide layer formed on the poly-Si on the contact electrodes of the μSEA. This difference—i.e. presence of titanium silicide at the sensing electrodes and absence at the contact electrodes—can be addressed to the difference in temperature between the relatively thin ($<$20 μm) silicon sieving structure and the bulk silicon substrate (525 μm) onto which the contact electrodes are located. During the RTP1 process of 700 °C and 750 °C, the temperature is raised rapidly (50 °C s^{-1}) to form $TiSi_2$, however, most likely the temperature of the contact electrodes does not reach the required silicidation temperature of 700 °C. Failed attempts to obtain C49-phase $TiSi_2$ on the sensing electrodes at RTP1 temperatures of 550 °C and 650 °C suggest that the temperature at the contact electrodes also stays below 650 °C, which indicates a difference between the sieving area and the bulk-Si area of 50 °C at a RTP1 of 700 °C. A heatsink effect is not uncommon for such micromachined membrane structures [35], modeling of the thermal profile also

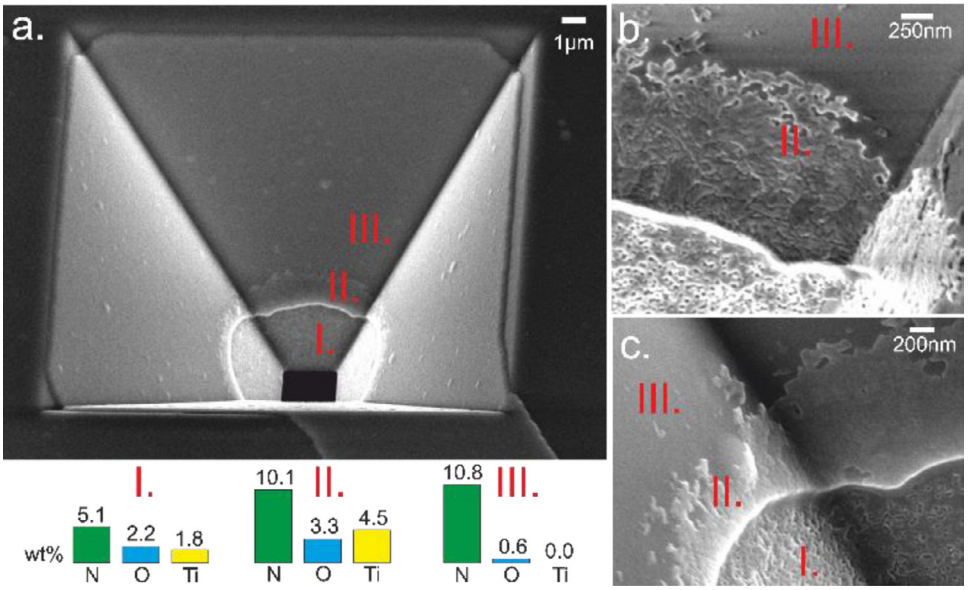

Figure 7. Scanning electron microscopy images with EDX analyses of a pore after the formation of titanium silicide by a RTP-1 at 700 °C and RTP-2 of 850 °C. The EDX analyses show titanium traces at the boron doped poly-Si sensing electrode (I), unexpected titanium traces on the SiRN at the lower region of the pore wall (II) and no titanium traces on the SiRN at higher regions of the pore wall (III) in (a)–(c). The zoom-in of the unexpected titanium silicide compound (II) shows the morphology of poly-Si and reveals grain boundaries (b). Electron beam voltage: 10 kV (a) and (c), 1.6 kV (b). The results of the EDX analyses for locations (I)–(III) are indicated for the elements nitrogen, oxygen and titanium. The silicon element is not shown in this figure, yet the values are resp. 90.9, 82.1 and 88.6 wt%.

shows a temperature difference of 50 °C between the sieving structure and bulk-Si (data not shown).

Another explanation for the presence or absence of $TiSi_2$ on the sensing and contact electrodes is the used heating source and its effect on the (1 1 1)-Si orientation of the pore walls (sensing electrode) in comparison to the (1 0 0)-Si orientation of the contact electrodes. Assumed is that the near infrared radiation used in the RTP process is transmitted through the substrate upon illumination when perpendicular to the (1 0 0)-Si plane at temperatures below 800 °C [36]. In case of surface roughness, here the (1 1 1)-Si planes of the pores, significantly more light, and thus heat, is absorbed [37]. In addition, the presence of the highly boron doped electrode layer also adds to this increased light absorption. This assumption is supported by EDX measurements at the SiRN on the pore walls, which indicated that an unexpected titanium silicide compound was formed during the salicide process (figure 7), which was limited to solely the pore walls. More precise, titanium silicide compounds are formed on SiRN at the pore wall, and most of this unexpected silicide compound is formed just above the sensing electrode (i.e. in the low region of the pore). The amount of unexpected titanium compound that is formed on the SiRN-coated pore walls scales with the pore aperture, and thus inherently depends on the sieving structure thickness. More specific, the height along the pore wall (starting from the aperture) up to which this titanium compound appears increases for larger the pore apertures.

The identification of this unexpected titanium silicide compound is based on the RCA-1 etch (excluding the hereby dissolved species: titanium, titanium oxide and titanium nitride) and literature [38]. Titanium-rich silicide (Ti_5Si_3) and TiSi are possible candidates. The formation of these silicides is mainly observed as a problematic feature at temperatures of $\geqslant$600 °C in the fabrication of gate electrodes using $TiSi_2$ [39]. From our experiments, this unexpected titanium silicide compound seems to be formed on the pore walls at RTP-1 temperatures as low as 550 °C, under both nitrogen and forming gas, while Ti_5Si_3 and TiSi formation is reported for a 600 °C RTP in an argon ambient and not a nitrogen ambient [39]. This also supports our assumption that the pore walls reach significantly higher temperatures compared to the RTP temperature settings (including the temperature measured by internal thermocouple in the RTP system).

Analysis by SEM show that this titanium silicide compound (formed on the SiRN) has the morphology of poly-Si and reveals grain boundaries. This is an indication for the formation of the unexpected titanium silicide, for which a silicon donor is needed. Thus, atomic reorganization of the excess silicon content of the low stress silicon-rich silicon nitride (SiRN) layer seems to account for the formation of a layer of unexpected titanium silicide.

The formation of the unexpected titanium silicide compound could not be prevented, since it is formed at lower temperatures compared to the aimed C54–$TiSi_2$ on the doped poly-Si. Yet no electrode short-circuiting nor enlarged noise of sensing electrodes can occur, despite the fact that these titanium silicides compounds have conductive properties, since they can be considered as a 'floating electrode' part. This assumption is based on the fact that this unexpected titanium silicide compound is not connected to the target titanium silicide formed on the poly-Si surface (sensing electrode), because of differences in height of the poly-Si and SiRN on the pore walls. More specific, the SiRN on top of the poly-Si has a thickness of 160 nm and the unexpected silicide does not bridge this 'height gap'. Since

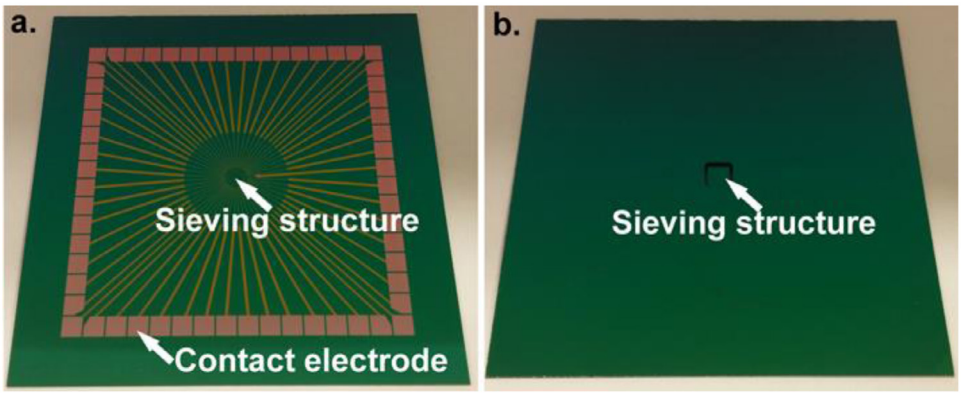

Figure 8. Photos of the final μSEA with a footprint of 49 $\times$ 49 mm. The front side of the μSEA (a), presenting the contact electrodes, lead wires and the sieve structure featuring the pores with integrated sensing electrodes. All electrode material consists of boron doped poly-Si, the lead wires are isolated with a silicon nitride layer, while the sensing electrodes are provided with a titanium silicide layer. The back side of the μSEA (b), showing the sieving structure originating from deep anisotropic back-etching of the silicon substrate.

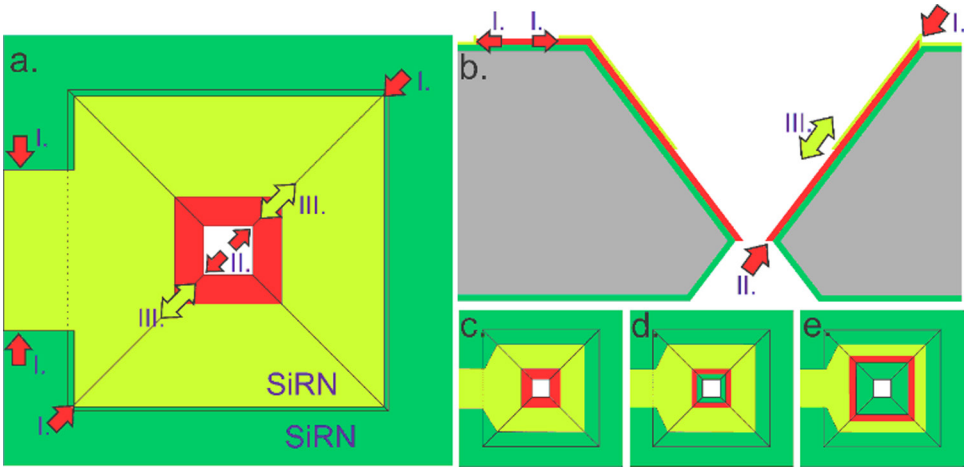

Figure 9. Schematic illustration of the tuning of the size and shape of the sensing electrode. The sensing electrode (red) is realized on the (1 1 1)-planes of an anisotropic etched inverted pyramidal shaped pore, which is insulated by a SiRN layer (green). The options for tuning its dimensions (top view: (a), side view: (b)) arise from two wet etch steps in the μSEA fabrication process. In both steps, (sacrificial) poly-Si is time-stopped under-etched, which either allows for tuning the poly-Si electrode layer (ET_1, indicated by red color) or functions as a mask layer for the removal of the SiRN insulation (ET_2, indicated by light-green). During ET_1, the poly-Si electrode layer is etched starting at the pore entrance and pore aperture (indicated by (I) and (II); red arrows). With respect poly-Si electrode layer, during ET_2, the sacrificial poly-Si is etched along the pore walls starting from the pore aperture and allows the removal of the SiRN insulation layer (indicated by (III); green arrows). Examples of possible electrode sizes and shapes according to the etching parameters (I)–(III) are provided in (c)–(e).

the formation of the unexpected silicide compound cannot be prevented and because it does not negatively affect the sensing electrode, further analysis of this compound is not performed.

After the formation of, presumably, the C54-phase titanium silicide on the poly-Si at the sensing electrodes by a second RTP (850 °C), dicing of the μSEA is performed. A footprint of 49 mm $\times$ 49 mm is realized, which is in agreement with the dimensions of a commercial Micro Electrode Array readout system (Multi Channel Systems, Reutlingen, Germany). Post to dicing and the removal of the dicing foil, the μSEA is finalized (figure 8) and ready for cell experiments.

3.5. Size and shape of the poly-Si sensing electrode in the μSEA

The electrode size and shape (i.e. the amount of surface area) for three fabricated μSEAs varied despite that all three have undergone the same fabrication process, except for the etch times during poly-Si electrode patterning, referred to as the 'first time-stopped etch step' and removal of SiRN insulation referred to as the 'second time-stopped etch step'. As a consequence, differently sized electrodes and electrode shapes are obtained.

The first time-stopped etch step (ET_1) comprises the patterning of the poly-Si (figures 9(a) and (b), indicated by (I) and (II); red arrows). In more detail, the poly-Si layer is patterned with the use of an oxide mask layer. After oxide patterning, the poly-Si electrode layer is under-etched along the pore walls from both the pore entrance (figures 9(a) and (b), indicated by (I)) as well as the pore aperture (figures 9(a) and (b), indicated by (II)). Thus, the duration of this poly-Si etch step determines the removal of electrode material related to the mask design. Although this etch step can be used to reduce the electrode size in the pore, its use is restricted, as the less significant contact electrodes (2200 μm in width) and more significant wires (10 μm in width) are etched as well (figures 9(a) and (b), also indicated by (I), not on scale).

Table 1. μSEA device specifications.

Device	Aperture length (μm)	ET_1 for poly-Si patterning (s)	Poly-Si layer A_1 (μm^2)	ET_2 for sensing electrode (min)	Sensing electrode A_2 (μm^2)
A	1.9	90	249.4	10	3.1
B	2.4	50	270.3	10	18.5
C	2.2	75	242.0	20	32.3

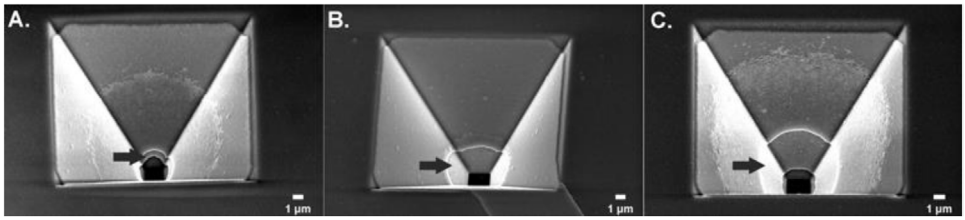

Figure 10. SEM images of pores containing a sensing electrode for three μSEAs (A)–(C). The sensing electrode surface area (arrow) is related to the etch times of the poly-Si electrode material and the SiRN insulation layer atop, which allows to tune the size and shape of the electrodes among different μSEAs.

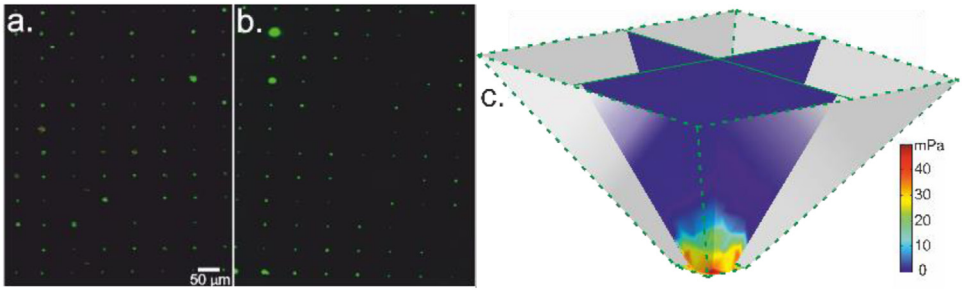

Figure 11. The positioning density of cortical neurons (a) and SH-SY5Y cells (b) was studied by counting cells in the pores after fluorescence staining. The shear stress inside a pore at 0.1 ml min^{-1} as modeled with COMSOL software (c).

The second time-stopped etch step (ET_2) comprises the removal of the SiRN insulation layer by sacrificial layer wet etching (figures 9(a) and (b), indicated by III; green arrows), which is explained in more detail in section 2.3. Summarized, the sacrificial poly-Si layer is under-etched to define the removal of SiRN from the doped poly-Si on the pore wall. This process starts from only the pore aperture and results in the final size of the sensing electrode, and thus the electrode surface for recording.

Although both these time-stopped etch steps are performed at different points during fabrication, it is clear that they are related. As a result, the sensing electrode surface will always be at a location in the lower part of the pore (i.e. close to the aperture). This feature not only allows for tuning the size of the sensing electrode, but also the shape and its location in respect to the pore aperture. Various optional sensing electrode shapes, sizes and locations are provided in figures 9(c)–(e).

The etch times and the resulting electrode surface area (A_1 and A_2) from ET_1 and ET_2 are provided in table 1, the resulting shapes of the sensing electrodes are shown in figure 10.

The electrode dimensions of the three analyzed μSEAs (A, B and C). For each μSEA the dimension of the pore aperture is given. Furthermore, the etch times for the first and second timed-stopped etch (ET_2 and ET_2) and the resulting poly-Si layer surface area (A_1) on the pore walls and the surface area of the sensing electrode (A_2) are given.

Clearly, it can be seen that the size and shape of the sensing electrodes can be varied by altering the etch times of the poly-Si and SiRN. The shape of the sensing electrode can be either a 'bucket' or a 'band' in the low region of the pore. Moreover the sensing electrode surface area can be tuned from a few square microns to several tens of square micrometers.

The option of tuning the electrode shape, location and size per μSEA is highly beneficial for obtaining the best signal recordings for a specific neuron/cell type. Here, transducer neurons, or other electrogenic cells, which are positioned in the pores need to be in intimate contact with the sensing electrode. The location where the cell is positioned in the pore mainly depends on the cell size, which can greatly differ between cell types and the origin of the mammalian species. Thus, it is valuable to be able to fine-tune the exact electrode location and size according to the cell size.

3.6. Positioning of μSEA transducer neurons

First experiments for positioning the transducer neurons on the 3D electrodes were performed. For the seeding efficiency, of the 1000 cells used, successful positioning was achieved for approximately 70% of cortical cells ($n = 3$) and approximately 80% for SH-SY5Y ($n = 3$) at a flow rate of 0.1 ml min^{-1} (figures 11(a) and (b)). Hence, to explore the influence of shear stress on cell viability, cortical neurons

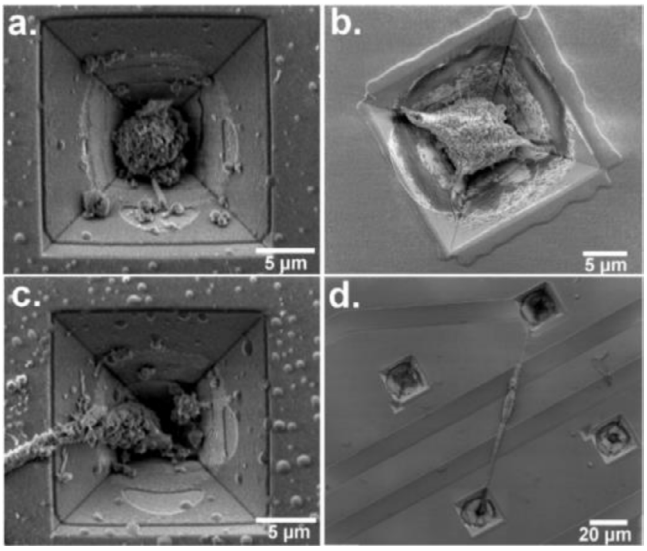

Figure 12. Scanning electron microscopy images of cortical neurons (14 DIV) (a) and (c) and SH-SY5Y cells (7 DIV) (b) and (d). Both cell types show a round morphology and are positioned and adhered in the pore.

were positioned at 0.1 ml min^{-1} and were stained for viability. Cortical cells were used, as these cells are considered to be the more vulnerable to shear stress compared to the SH-SY5Y. Counting of the stained cortical neurons shows a viability of 70%, which is in agreement with general cell culture experiments on tissue culture plates [15, 40]. This result indicates that shear stress in the pores of the μSEA has most likely no direct influence on cell viability, however, the effect on cell behavior has yet to be studied more thoroughly. The established COMSOL model of a single pore showed a shear stress of 4.6 mPa at the pore opening and 43.6 mPa at the aperture at a sieve flow rate of 0.1 ml min^{-1} (figure 11(c)), which is very low in comparison with neuron membrane disruptions of 14 Pa (for 30 s with a 0.50 strain) [41]. Furthermore, *in vivo* interstitial fluid flow regenerates shear stresses in the order of 0.5–1.5 mPa [42], whereas *in vivo* arterial vascular network shear stresses between 1 and 7 mPa are found [43]. Clearly, the exact shear stress exposure depends on the residence time of each individual cell at a certain location in the pore. To minimalize the shear stress exposure time, the cells should be seeded simultaneously at the end point of the applied suction. This is achieved by loading the reservoir with culture medium before the suction is applied. Hereby the cells are concentrated in a relatively small volume, to prevent the cells from adhering to the sieving structure before any suction is applied.

3.7. Culturing and analysis of μSEA transducer neurons

For the rat cortical neurons (14 DIV) and SH-SY5Y cells (7 DIV), SEM images confirmed neuron adhesion to the pore walls (figures 12(a) and (b)) and the cells exhibit a round morphology, similar to cortical cells cultured in 3D environments [44]. Due to the difference in size of these cells, their adhesion location in the pore is different, for which the tuning of the sensing electrode surface and location is useful. Also, SEM observations display initial neuron processing, the formation of cell protrusions which predicts cell viability and functioning of both cell types. The formation of protrusions is found to be different for the cell types. Rat cortical cells showed a minor formation of protrusions (figure 12(c)), while the SH-SY5Y cells already formed connections between neurons (figure 12(d)). This difference can be explained by the origin of both cell types and their rate of metabolism, as the rat cortical cells are primary cells whereas the SH-SY5Y cells are a cloned cell model derived from a cancerous cell line. It is important to mention that both cell types behave as intended, including minimal or no reciprocal network formation between the pores, as their function is to form the neuroelectronic interface for the 3D culture atop.

In line with this observation of minimal network formation, due to the low cell densities used in the cortical and SH-SY5Y cell studies, rat hippocampal cells were plated (i.e. without suction) at a higher density compared to the rat cortical and SH-SY5Y cells. This experiment allows to study the development and network on the μSEA surface. Microscope observations show that hippocampal cells were positioned in the pores and on the planar surface in between the pores of the μSEA. Within 3 DIV the cells were adhered onto the planar surface and network formation was initiated. At 7 DIV–21 DIV the network was further densified and reorganization was observed. The development of the cells positioned in the pores was not visible with a light microscope at relatively low magnifications. Nevertheless, it is assumed that pores occupied with cells block the passing light, resulting in the observation of dark pores (figures 13(a)–(c)). Observations show that these cells reside in the pores and maintain their position during the 21 d of culturing. This also indicates that cell migration from the pores to the planar surface is not encouraged, assuming that the cells in the pores are still viable during the culturing.

Although extended long-term cultures and reproducibility of positioning efficiency related to shear stress and viability have to be studied, the initial results provide sufficient evidence to support the use of the μSEA for future neuroelectrophysiological applications.

3.8. μSEA electrical characterization

The three μSEAs (devices A, B and C) have been used for the electrical characterization of the sensing electrodes. The baseline noise of all tested μSEA devices is below 15 μV, which is sufficiently low to distinguish amplitude changes up to 100 μV during the recording of neuronal activity. In comparison, commercially available planar TiN microelectrode arrays show a baseline noise of approximately 8 μV [45]. A signal input of 100 mV at 1 kHz was selected as the basis for comparison to reported MEA devices in literature. Reported impedance values of TiN and ITO coated electrodes are 30–50 kΩ for an electrode surface of 706.9 μm^2 and 250–400 kΩ for an electrode surface of 78.5 μm^2, respectively [45].

Impedances of polycrystalline silicon thin-film porous sensing electrodes (20 μm in diameter) reported in literature are 100 kΩ without native oxide and 500 kΩ with native oxide [46].

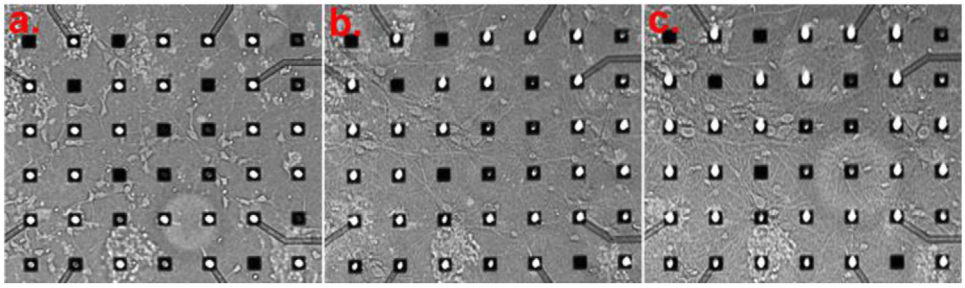

Figure 13. Hippocampal cells (60 000 cells) were positioned in the pores (dark squares) and onto the planar surface in between the pores to study cell development and network formation for 3 DIV (a), 7 DIV (b) and 21 DIV (c). Image courtesy of D Ito and M Chiappalone of the Istituto Italiano di Tecnologia.

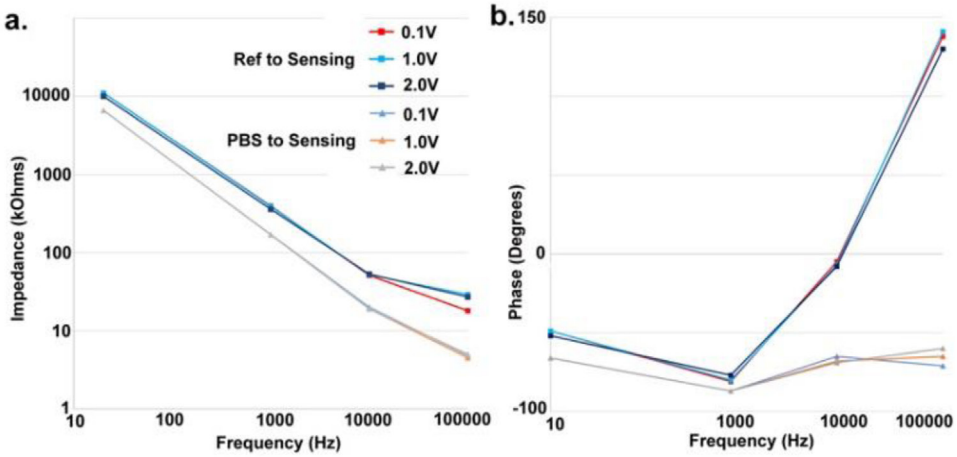

Figure 14. Impedances (a) and phase shift (b) measured between a sensing electrode and the reference electrode (Ref to Sensing) and PBS and a sensing electrode (PBS to Sensing) of μSEA C at different amplitudes.

For the μSEA, impedance measurements are done between a sensing electrode and the reference electrode with the addition of PBS (Ref to Sensing). In case of μSEA C, an impedance of approximately 360 kΩ, with a phase shift of $-78°$, was obtained. Comparable values for the used amplitudes were obtained for both the impedance and phase, indicating a linear system in the range of 100 mV–2 V. In detail, the impedance as a function of the frequency shows a logarithmic linear decrease (figure 14(a), Ref to Sensing) and displays capacitive behavior for low frequencies (10 Hz–8 kHz, Ref to Sensing) and resistive behavior for higher frequency range (10 kHz–100 kHz) (figure 14(b), Ref to Sensing).

The obtained impedances are roughly identical for all three indicated μSEAs (A, B and C), which is rather peculiar since their sensing electrode surface areas are different. This might indicate an electrical leakage of the insulation layers due to which the electrical system behaves like a parallel combination rather than a serial combination of RC circuit elements. To exclude the presence of leakage, resistance measurements were performed upon applying a DC-potential of 21 V. Hereby the reference electrode was connected to the sensing electrode, which displayed an infinite resistance. Upon filling the PDMS reservoir with PBS, a resistance of 7 MΩ was obtained, which indicates the absence of leakage or short-circuitry of the SiRN layers.

The integrated single reference electrode has a surface area of 0.22 mm^2, whereas the four reference electrodes in commercial TiN MEA (120MEA series, MultiChannelSystems GmbH, Reutlingen, Germany) have a surface area of 8.4 mm^2 each. This could potentially mean that the reference electrode included in the μSEAs affects the magnitude of the total measured impedance, in addition to the sensing electrode, and thus influence the charge transfer on basis of a double layer capacitance and/or polarization at the reference electrode. To proof this hypothesis, the interference of the reference electrode on the impedance measurements is avoided by connecting the PBS droplet directly to the sensing electrode (PBS to Sensing). To do so, the tip of a microprobe with a surface of 1.52 mm^2 is brought into the PBS solution. First, a measurement without the addition of the PBS for Ref to Sensing shows an impedance of around 3.6 MΩ with a phase shift of approximately 0° for 100 mV at 1 kHz. After the addition of PBS, the PBS to Sensing measurements of μSEA C, an impedance approximately 170 kΩ with a phase shift of $-67°$ was found for 100 mV at 1 kHz. The impedance as a function of the frequency shows a logarithmic linear decrease (figure 14(a), PBS to Sensing) and shows capacitive behavior for the full frequency range (10 Hz–100 kHz) (figure 14(b), PBS to Sensing). The obtained impedance values for the PBS to Sensing measurements are lower compared to the Ref to

Sensing, yet their profile is approximately identical. This indicates that the reference electrode contributes to roughly the half of the Ref to Sensing measured impedance, while the reference electrode influence is expected to be insignificant with the lowest impedance possible.

To fully understand the nature of the μSEA's complex electrical circuit, more technical parameters have to be taken into account, including the magnitude of the charge transfer, the double layer capacitance and polarization of the sensing electrode. Thus further electrical analysis is required to make conclusive decisions on the (in)correct electrical behavior for neuronal recordings using the μSEA devices. Yet the measured impedance values obtained seem to potentially allow for the measurement of single cell recordings, in agreement with the impedance value of at most 500 kΩ stated in literature [47].

4. Conclusions

A μSEA for electrophysiological measurements supporting the generation of a complete 3D culture of neuronal cells is fabricated. In this work we demonstrate that poly-silicon is successfully patterned, doped and isolated on both the (1 0 0)-Si and (1 1 1)-Si planes. A lithography concept has been developed, based on the physical connection of the top and bottom side of the sieving structure combined with sacrificial layer etching. This concept is used for the selective removal of the isolation layer from electrodes and allows for the tuning of the final electrode size and shape. The hereby exposed boron doped poly-silicon sensing electrodes are provided with a titanium silicide (C54-phase $TiSi_2$) coating that has a lower oxidation rate than poly-Si, thereby providing and maintaining a low resistance contact between the neuron and the electrode. The fabrication process allows for the tuning of the sensing electrode position and shape on the pore walls and the sensing electrode surface area by varying the etch times, which is beneficial to obtain optimal coupling between cell and electrode in case of different cell types. This is demonstrated by positioning of different transducer neuron types (cortical and SH-SY5Y cells) in μSEAs. A cross flow over the microsieve has been proven to be successful in terms of efficiency and viability. Transducer neurons, from cortical rat neurons and SH-SY5Y, are successfully positioned into the pores of the μSEA and show initial neuronal processes. Hippocampal cells plated and cultured on the μSEA surface are developing neurites and form neuronal networks. These results show that the μSEA includes a bio-friendly environment, which supports the culturing of different transducer neurons. Furthermore, a simulation model indicates a relatively low shear stress at the aperture, which supports the observed survival of cells after positioning. Electrical characterization of the sensing electrodes in the μSEA shows an impedance value and baseline noise level that are sufficiently low compared to literature. Although the initial electrical characterization indicates the successful use of the μSEA for electrophysiological measurements, the actual electrophysiology studies still need to be performed. These electrophysiology studies and potential optimization of the μSEA is expected in the near future.

Acknowledgments

This project is financially supported by the ERC, Starting Grant no. 280281 (MESOTAS). The authors thank J P Frimat from the Eindhoven University of Technology for his work on the SH-SY5Y cells, and M Chiappalone and D Itoh of the Istituto Italiano di Tecnologia for their work on the hippocampal cells. We thank from the University of Twente, J W Berenschot for the theoretical support, W J C Vijselaar for his work on the IBE and H-W Veltkamp for the COMSOL modeling.

References

[1] Obien M E, Deligkaris K, Bullmann T, Bakkum D J and Frey U 2015 *Front. Neurosci.* **8** 423
[2] McConnell E R, McClain M A, Ross J, LeFew W R and Shafer T 2012 *Neurotoxicology* **33** 1048–57
[3] Scelfo B, Politi M, Reniero F, Palosaari T, Whelan M and Zaldívar J M 2012 *Toxicology* **299** 172–83
[4] Dunlop J, Bowlby M, Peri R, Vasilyev D and Arias R 2008 *Nat. Rev. Drug Discov.* **7** 358–68
[5] Spira M E and Hai A 2013 *Nat. Nanotechnol.* **8** 83–94
[6] Valero A, Merino F, Wolbers F, Luttge R, Vermes I, Andersson H and van den Berg A 2005 *Lab Chip* **5** 49–55
[7] Tan W H and Takeuchi S 2007 *Proc. Natl Acad. Sci. USA* **104** 1146–51
[8] Kobel S, Valero A, Latt J, Renaud P and Lutolf M 2010 *Lab Chip* **10** 857–63
[9] Tonomura W, Moriguchi H, Jimbo Y and Konishi S 2008 *Int. Conf. of the IEEE Engineering in Medicine and Biology Society* pp 943–6
[10] Suzuki K, Tanabe M, Ezaki T, Konishi S, Oka H and Ozaki N 2005 *Trans. Inst. Electron. Commun. Eng. Japan* E **125** 216–221
[11] Martinez D, Py C, Denhoff M W, Martina M, Monette R, Comas T, Luk C, Syed N and Mealing G 2010 *Biomed. Microdevices* **12** 977–85
[12] Alberti M, Snakenborg D, Lopacinska J M, Dufva M and Kutter J P 2010 *Microfluid. Nanofluid.* **9** 963–72
[13] Yobas L 2013 *J. Micromech. Microeng.* **23** 083002
[14] Shimba K, Sakai K, Isomura T, Kotani K and Jimbo Y 2015 *Integr. Biol.* **7** 64–72
[15] Wheeler B C and Brewer G J 2010 *Proc. IEEE Inst. Electr. Electron. Eng.* **98** 398–406
[16] Scott A, Weir K, Easton C, Huynh W, Moody W J and Folch A 2013 *Lab Chip* **13** 527–35
[17] Knight E and Przyborski S 2015 *J. Anat.* **227** 746–56
[18] Frega M, Tedesco M, Massobrio P, Pesce M and Martinoia S 2014 *Sci. Rep.* **4** 5489
[19] Berenschot E J *et al* 2012 *Small* **8** 3823–31
[20] Schurink B, Berenschot J W, Tiggelaar R M and Luttge R 2015 *Microelectron. Eng.* **144** 12–8
[21] Schurink B and Luttge R 2013 *J. Vac. Sci. Technol.* B **31** 06F903
[22] Chen F W, Tjahjono B S, Guo J H, Cousins P J and Cotter J E 2003 *Proc. Solar—Australian and New Zealand Solar Energy Society*
[23] Mann R W, Clevenger L A, Agnello P D and White F R 1995 *IBM J. Res. Dev.* **39** 403–17
[24] Romijn H J, Van Huizen F and Wolters P S 1984 *Neurosci. Biobehav. Rev.* **8** 301–34

[25] Frimat J P, Xie S, Bastiaens A, Schurink B, Wolbers F, den Toonder J and Luttge R 2015 *J. Vac. Sci. Technol.* B **33** 06F902
[26] Frega M, Pasquale V, Tedesco M, Marcoli M, Contestabile A, Nanni M, Bonzano L, Maura G and Chiappalone M 2012 *Neurotoxicol. Teratol.* **34** 116–27
[27] Lee J T Y and Chow K L 2012 *Scanning* **34** 12–25
[28] Thompson C V 2012 *Annu. Rev. Mater. Sci.* **42** 399–434
[29] Berenschot E, Tas N R, Jansen H V and Elwenspoek M 2008 *3rd IEEE Int. Conf. on Nano/Micro Engineered and Molecular Systems NEMS* pp 729–32
[30] Abba A, Galerie A and Caillet M 1982 *Oxid. Met.* **17** 43–54
[31] Amano J, Merchant P, Cass T R, Miller J N and Koch T 1986 *J. Appl. Phys.* **59** 2689–93
[32] Lee H G 1992 *Thin Solid Films* **216** 230–4
[33] Bartur M and Nicolet M A 1984 *J. Electrochem. Soc.* **131** 371–5
[34] Ponpon J P and Saulinier A 1990 *Appl. Surf. Sci.* **40** 315–8
[35] Tiggelaar R M, Loeters P W H, Van Male P, Oosterbroek R E, Gardeniers J G E, De Croon M H J M, Schouten J C, Elwenspoek M C and Van den Berg A 2004 *Sensors Actuators* A **112** 267–77
[36] Cullen C W and Sturm J C 1995 *IEEE Trans. Semicond. Manuf.* **8** 346–51
[37] Timans P J, Sharangpani R and Thakur R P S 2000 *Handbook of Semiconductor Manufacturing Technology* ed Y Nishi and M Dekker (New York: CRC Press)
[38] Morgan A E, Broadbent E K, Ritz K N, Sadana D K and Burrow B J 1988 *J. Appl. Phys.* **64** 344–53
[39] Brat T, Osburn C M, Finstad T, Liu J and Ellington B 1986 *J. Electrochem. Soc.* **133** 1451–8
[40] Xie S and Luttge R 2014 *Microelectron. Eng.* **124** 30–6
[41] LaPlaca M C, Cullen D K, McLoughlin J J and Cargill R S 2005 *J. Biomech.* **38** 1093–105
[42] Scallan J, Huxley V H and Korthuis R J 2010 *Colloquium Lectures on Integrated Systems Physiology* (San Rafael, CA: Morgan and Claypool)
[43] Malek A M, Alper S L and Izumo S 1999 *JAMA* **282** 2035–42
[44] LaPlaca M C, Vernekar V N, Shoemaker J T and Cullen D K 2010 Three-dimensional neuronal cultures *Methods in Bioengineering: 3D Tissue Engineering* ed F Berthiaume and J Morgan (Norwood, MA: Artech House) pp 187–204
[45] Lawand N S, French P J, Briaire J J and Frijns J H M 2012 *Proc. Eng.* **47** 726–9
[46] Bucher V, Graf M, Stelzle M and Nisch W 1999 *Biosens. Bioelectron.* **14** 639–49
[47] Potter S M 2001 *Prog. Brain Res.* **130** 49–62